ACS OMEGA

Open Access

http://pubs.acs.org/journal/acsodf

Article

Nonadiabatic Effects in the H + LiD(v = 0, j = 0) → Li(2s) + HD Reaction Near Cold Collisions

Yuwen Bai,* Bayaer Buren, and Zijiang Yang*

Cite This: *ACS Omega* 2025, 10, 5934−5942

Read Online

ACCESS | Metrics & More | Article Recommendations

ABSTRACT: Nonadiabatic dynamic study of the H + LiD(v = 0, j = 0) → Li(2s) + HD reaction is carried out using the time-dependent wave packet method in a collision energy range of 1−80 cm^{-1}. The total integral cross section exhibits a partial wave resonance near 2 cm^{-1}, corresponding to the opening of the J = 5 partial wave. The nonadiabatic coupling effects inhibit the reactivity, especially for the low-vibrational states. The rotational excitation of products is affected by nonadiabatic coupling effects. The maximum accessible rotational state of the products is higher when nonadiabatic effects are included than when they are omitted. At low collision energies, the product angular distributions are influenced by the resonances. Nonadiabatic results reveal a more pronounced backward scattering of the products than adiabatic results. As collision energy increases, the stripping mechanism gradually becomes dominant, and both adiabatic and nonadiabatic results exhibit significant forward-scattering characteristics.

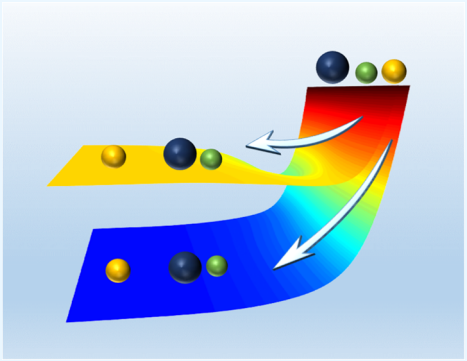

1. INTRODUCTION

Molecular dynamics emerged and flourished with the advancement of computers and experimental instruments, enabling a detailed understanding of chemical reactions. In the theoretical study, the Born−Oppenheimer (BO) approximation, which ignores the coupling between electrons and nuclei, is based on the assumption that nuclear motion is much slower than electronic motion. In most systems, the BO approximation facilitates the calculation of dynamics, while in some systems, the nonadiabatic effects caused by the coupling between electrons and nuclei play an important role in the reaction process. Therefore, the study of nonadiabatic coupling is very meaningful in these systems.[1−9]

Nonadiabatic coupling is often associated with avoided crossings or conical intersections (CIs) between two potential energy surfaces (PESs). However, the impact of nonadiabatic coupling is not limited to the vicinity of crossings. In a reaction, nonadiabatic effects at different collision energies may exhibit similar or different behaviors. Geometric phase (GP) effects are a type of nonadiabatic effect related to CIs. H + H_2 and its isotopologue reactions are used as examples. Geometric phase effects manifest in the reaction once the collision energy surpasses the CI threshold. Yuan et al. performed both high-resolution crossed molecular beam experiments and theoretical studies of the H + HD reaction at a collision energy slightly above the CI.[10] They observed fast angular oscillations in the differential cross sections (DCSs) of the H_2 product and found that theoretical calculations matched experimental results only when GP effects were included. In 2008, Bouakline et al. showed that the reaction probability exhibits a strong GP effect at collision energies above 3.5 eV.[11] Additionally, GP effects in these reactions also have been studied extensively when the collision energy is much lower than CI. In their study of the H + HD reaction at collision energies ranging from 1.94 to 2.21 eV, Xie et al. observed notable oscillation patterns resulting from quantum interference between direct abstraction and roaming insertion pathways.[12] In 2005, the study showed that there are no GP effects for the H + H_2 reaction when collision energy is lower than 1.8 eV.[13] However, two distinct phenomena have been observed: shifts in the DCS peak for the H + D_2 reaction at 1.42 eV[14] and forward-scattering oscillations in the H + HD reaction at a collision energy of 1.35 eV.[15] Additionally, GP effects have been found in rotationally resolved DCSs for the H + H_2 and its isotopologues reactions at the ultracold collision energy range.[16−19] These findings underscore the necessity to study nonadiabatic coupling effects across different collision energies. In recent years, there has been a significant amount of research on nonadiabatic studies involving chemical reactions that include alkali metals, such as Na + NaLi,[20] Rb + KRb,[21] K + H_2,[22−24] Na + H_2/HD,[25−28] H + Li_2[29] and Li + H_2[30−35] reactions. Many valuable phenomena have been discovered.

Received: October 29, 2024
Revised: January 21, 2025
Accepted: January 28, 2025
Published: February 4, 2025

In LiH_2 systems, reactions involving H + LiH and its isotopologues are exothermic, making them suitable for studying nonadiabatic effects at low temperatures. These reactions have attracted the interest of researchers.[36−38] Li et al. applied the time-dependent wave packet (TDWP) method to study the nonadiabatic dynamic of the H + LiH reaction in the collision energy range of 0.001−0.1 eV.[39] It was discovered that the nonadiabatic effects exhibit a significant impact, particularly at low J values. This finding emphasizes the importance of considering the nonadiabatic effects when analyzing the H + LiH reaction under investigation. In their follow-up study,[40] they studied how nonadiabatic effects influence the reaction rate constant. Their findings demonstrated that omitting nonadiabatic effects substantially overestimates the rate constant, with these effects being most pronounced in low-vibrational states. In our previous study of the H + LiD(ν = 0, j = 0) reaction at collision energies between 0.1 and 0.5 eV, we focused on analyzing both the ground state product channels and the hydrogen exchange reaction pathways due to the higher zero-point energy of the excited state compared to that of the ground state. Several interesting phenomena have been found.[41] After considering the nonadiabatic effects, reaction reactivity decreases and more products are excited to high vibrational excited states. Additionally, our results showed that the differences between the adiabatic and nonadiabatic values are substantial at low collision energies. Based on the above analysis, nonadiabatic couplings may have an effect at different collision energies. This work aims to study the influence of nonadiabatic effects on this reaction near low temperatures. Additionally, considering the results from our previous studies that show nonadiabatic effects have a substantially greater impact on the formation of ground state Li products compared to exchange processes, as well as the zero-point energy of the exchange channel, we decided to investigate the ground state product channels.

In this work, we report a detailed investigation of the nonadiabatic dynamics of the H + LiD(ν = 0, j = 0) → Li(2s) + HD reaction based on the accurate PESs, which is developed by He et al.[42] over a collision energy range of 1−80 cm^{-1}. To study nonadiabatic processes, the (quasi) static picture provided by the time-independent Schrödinger equation within the BO approximation is no longer applicable, instead, full-time-dependent electronic and nuclear quantum problems need to be solved.[43] The nonadiabatic effects are generally studied in the diabatic representation, where the accuracy of dynamic results mainly depends on the accuracy of the diabatic potential energy matrix, indicating that an accurate dynamic method is required to calculate the nonadiabatic effects. We used the improved TDWP method to calculate the dynamics. The remainder of this paper is organized as follows: Section 2 provides a brief introduction to the calculation method. Section 3 presents our results and related discussions. Section 4 presents the conclusions of this study.

2. THEORETICAL METHODS

The traditional wave packet methods face significant challenges in cold and ultracold collisions due to the large number of channels and the need for a vast number of grids to accommodate the long de Broglie wavelengths, leading to steep numerical calculations. The new improved L-shaped grid method used in this work was developed by Buren et al.[44] In the L-shaped grid method, the total scattering wave function is divided into two parts: the interaction region and the asymptotic region. Each region can be optimized to efficiently and accurately describe the reaction dynamics based on the characteristics of wave function evolution. The improved method reduces the computational load by using fewer rotational basis sets in the asymptotic region, where only elastic and inelastic scattered waves occur. This TDWP method overcomes the issue of high computational demands in traditional methods, making it suitable for calculations at low collision energies, which have been proven to be sufficiently accurate. Here, we provide a brief overview of this method as follows.

The total Hamiltonian in the reactant Jacobi coordinate (R, r, θ) can be written as

$$\hat{H} = \hat{T} + \hat{V} \tag{1}$$

where $\hat{V}$ is the reference potential energy operator, which can be obtained from the PES. The title reaction is associated with $1^2A'$ and $2^2A'$ states of the LiH_2 molecule in C_s symmetry. The diabatic wave functions can be derived from the adiabatic wave functions through the application of a unitary transformation. In this work, diabablizations based on molecular properties methods.[45,46] The transition dipole moments are used to obtain the diabatic potential energy matrix. $\hat{T}$ is the kinetic energy operator. In atom−diatom reactions, the $\hat{T}$ is given as

$$\hat{T} = -\frac{\hbar^2}{2\mu_R}\frac{\partial^2}{\partial R^2} + \hat{h}_r + \frac{\hat{j}^2}{2\mu_r r^2} + \frac{(\hat{J} - \hat{j})^2}{2\mu_R R^2} \tag{2}$$

where μ_R and μ_r are reduced masses of R and r coordinates, respectively. $\hat{J}$ is the total angular momentum operator, and $\hat{j}$ is the rotational angular momentum operator of the BC molecule.

The initial wave packet is the product of Gaussian wave packet $G(R)$ and initial rovibrational state wave function $\phi_{v_0 j_0}(r)$; the initial wave packet can be written as

$$\Psi^{JMP}_{av_0 j_0 l_0}(t = 0) = G(R)\phi_{v_0 j_0}(r)|JMj_0 l_0 P\rangle \tag{3}$$

the $G(R)$ is defined as

$$G(R) = \left(\frac{2}{\pi\delta^2}\right)^{1/4} \exp\left[-\frac{(R - R_0)^2}{\delta^2} - i\sqrt{2\mu_R E_0}R\right] \tag{4}$$

where R_0 and δ define the position and width of the initial wave packet, respectively. E_0 is the mean collision energy in the center of mass frame, and $|JMj_0l_0P>$ is the eigenfunction of the total angular momentum of the system in the space-fixed coordinates.

To facilitate the propagation of the wave packet, the wave packet is transformed from space-fixed coordinates to body-fixed reactant Jacobian coordinates. The wave packet is written as

$$\Psi^{JMP}(\boldsymbol{R}, \boldsymbol{r}, t) = \sum_{n,v,j,K} F^{JMP}_{nvjK}(t)u_n(R)\phi_v(r)y^{JMP}_{jK} \tag{5}$$

where $u_n(R)$, $\phi_v(r)$, and y^{JMP}_{jK} are the translational, vibrational, and rotational basis, respectively. The wave packet propagation is performed in the body-fixed representation using the second-order split-operator method.[47] The propagation process can be written as

https://doi.org/10.1021/acsomega.4c09864
ACS Omega 2025, 10, 5934−5942

$$\Psi(t + \Delta_t) = e^{-i\hat{V}\Delta_t/2} e^{-i\hat{T}_j\Delta_t/2} e^{-i(\hat{T}_R+\hat{h}_r)\Delta_t} e^{-i\hat{T}_j\Delta_t/2} e^{-i\hat{V}\Delta_t/2} \Psi(t) \quad (6)$$

After the propagation, the S-matrix that contains the dynamics information can be written as

$$S^J_{v_{f_f}j_f l_f \leftarrow v_0 j_0 l_0}(E) = \frac{1}{\alpha(E)} \sqrt{\frac{k_f}{2\pi\hbar^2\mu_{R_f}}} h_{l_f}(k_f R_{f\infty}) \langle \chi_{v_{f_f}j_f} | \Psi^+(E; R_{f\infty}) \rangle \quad (7)$$

where μ_{R_f} is the reduced mass at the product Jacobi coordinate, k_f is the wave vector in the product channel, h_{l_f} is the outgoing Ricatti-Hankel function, and $R_{f\infty}$ is the product scattering coordinate in the product asymptote. The $\alpha(E)$ is the amplitude of the initial wave function, and $\Psi^+(E; R_{f\infty})$ means Fourier transform.

The state-to-state integral cross sections (ICSs) are obtained by

$$\sigma_{v'j' \leftarrow vj}(E) = \frac{\pi}{(2j_0 + 1)k^2_{v_0 j_0}} \sum_{K'KJ} (2J + 1)|S^J_{v'j'K' \leftarrow vjK}(E)|^2 \quad (8)$$

the state-to-state DCSs are obtained by

$$\frac{d\sigma_{v'j' \leftarrow v_0 j_0}(\vartheta, E)}{d\Omega} = \frac{1}{(2j_0 + 1)} \sum_{K',K} \left| \frac{1}{2ik^2_{v_0 j_0}} \sum_J (2J + 1) d^J_{K'K}(\pi - \vartheta) S^J_{v'j'K' \leftarrow v_0 j_0 K} \right|^2 \quad (9)$$

where ϑ is the scattering angle, $k_{v_0 j_0}$ is the momentum in the entrance channel, and $d^J_{K'K}(\vartheta)$ is the reduced rotation matrix.

3. RESULTS AND DISCUSSION

In this work, a series of quantum adiabatic and nonadiabatic calculations are performed for the H + LiD(ν = 0, j = 0) → Li(2s) + HD reaction at collision energies ranging from 1 to 80 cm^{-1}. The dynamically calculated parameters and accuracy of the PESs are very important at such low collision energies. The initial wave packet is located at 60 a_0 in the TDWP calculation. The maximum R coordinate used is 300 a_0 with 3999 grids, and the maximum r coordinate used is 15 a_0 with 130 grids, which is sufficiently precise for this study to ensure convergence. Other data used are listed in Table 1. The HYLC PESs are very accurate nonadiabatic PESs of the LiH_2 system to date, ensuring the reliability of the results.

3.1. ICSs. The initial total ICSs of the H + LiD(ν = 0, j = 0) reaction is plotted in Figure 1 as a function of collision energy. The total ICS decreases sharply at first and then changes gently as the collision energy increases, which is consistent with the characteristics of exothermic reactions. The black and red lines represent the results of the nonadiabatic and adiabatic calculations, respectively. Figure 1 illustrates that the total ICS diminishes when considering the nonadiabatic effects. Therefore, the nonadiabatic effects cannot be ignored directly. There are oscillations on both curves, meaning that resonances exist at low collision energies (1−30 cm^{-1}). The resonance positions are identical in both adiabatic and nonadiabatic calculations, indicating that resonance formation is independent of nonadiabatic effects. To identify the resonance-related partial wave, the total ICS and cross sections for total angular momentum J = 0−5 are plotted in Figure 2. There are many oscillatory structures in the ICS curve. The most obvious resonance near 2 cm^{-1} is contributed by the J = 5 partial wave.

To verify the existence of resonance, we plotted the total scattering wave function for the reaction H + LiD → Li(2s) + HD at a total angular momentum quantum number of 5 and a collision energy of 2.4 cm^{-1}, as a function of $R_{H\text{-}LiD}$ and r_{LiD}, as shown in Figure 3. The enhancement of the wave function can be clearly seen in the figure, indicating the presence of a resonance in the reaction. This kind of resonance is caused by the opening of the single partial wave and always occurs at low collision energies. The partial wave resonance has been discussed in the research of S(^{1}D) + H_2[48] and H + LiH^+[49] reactions. While the resonance position and its associated partial waves remain unaffected by nonadiabatic effects, the resonance intensity is reduced, suggesting that nonadiabatic effects influence the resonance lifetime. In Figure 4, both adiabatic and nonadiabatic cross sections of total angular momentum J = 0 are shown. The rotational energy levels of the LiD(ν = 0) molecule are represented by dashed lines, where j is the rotational quantum number of the LiD. The ICS curves exhibit three resonance peaks. Two of these resonance peaks correspond to the rotational energy levels of LiD (ν = 0), indicating that the resonances in the H + LiD reaction are related to the quasi-bound states of H-LiD(j). Owing to the

Table 1. Main Parameters Used in TDWP Calculations for the H + LiD → Li(2s) + HD Reaction[a]

parameters	values
R	$R \in [0.01, 300.0]$
	N_R = 3999 (199 for interaction region)
r	$r \in [0.4, 15.0]$
	N_r = 130 (6 for asymptotic region)
θ	N_θ = 200 (10 for asymptotic region)
damping function for R	R_a = 100.0, R_b = 300.0, C_R = 0.01
damping function for r	r_a = 11.0, r_b = 15.0, C_r = 0.08
initial wave packet	R_0 = 60.0, δ = 4.0, E_0 = 0.005 eV
total propagation time	2,000,000 (J < 6), 1,000,000 (J > 7)
time step	Δ_t = 50
projection plane	$R_{f\infty}$ = 9.0

[a]Atomic units are used if not otherwise stated.

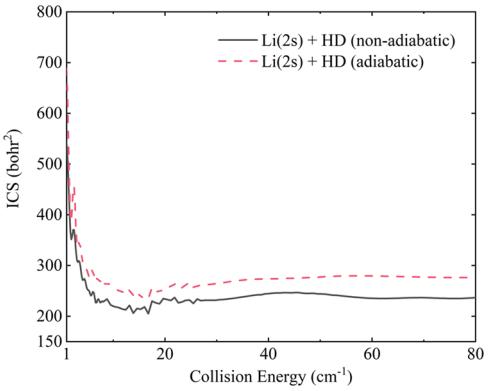

Figure 1. Total ICS for the H + LiD(ν = 0, j = 0) → Li(2s) + HD reaction as a function of collision energy in the adiabatic (red line) and nonadiabatic (black line) representation.

https://doi.org/10.1021/acsomega.4c09864
ACS Omega 2025, 10, 5934−5942

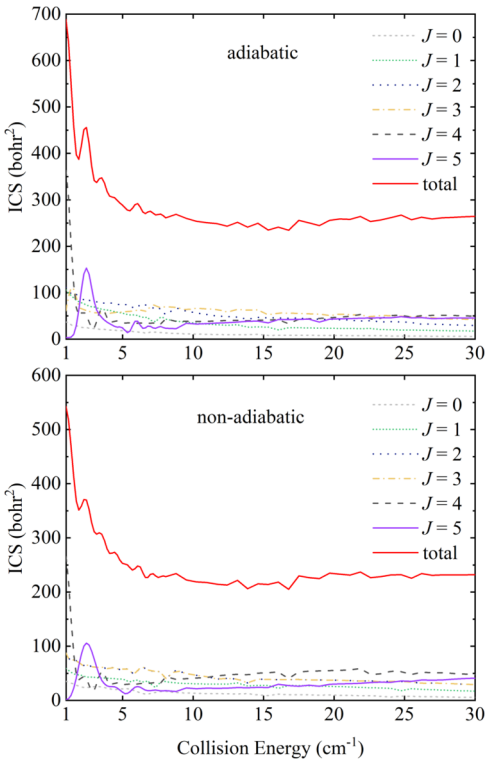

Figure 2. Cross sections for different total angular momentum and total integral cross section for the H + LiD(ν = 0, j = 0) → Li(2s) + HD reaction.

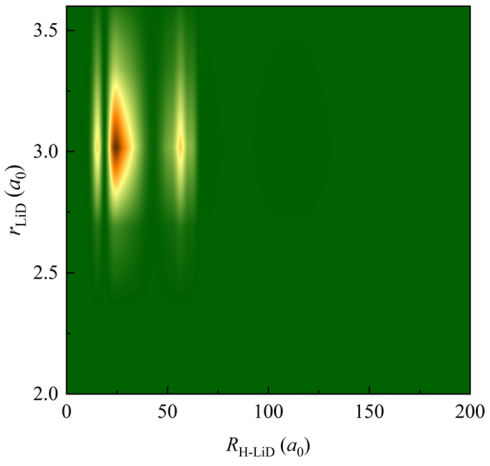

Figure 3. Total scattering wave function of H + LiD → Li(2s) + HD reaction at 2.4 cm^{-1} collision energy as a function of $R_{H\text{-}LiD}$ and r_{LiD} for J = 5.

effect of partial wave averaging, these resonances cannot be found in the total ICS.

In Figure 5, the nonadiabatic and adiabatic results for identical vibrational product states are represented by dashed and solid lines, respectively. The nonadiabatic ICS is lower than the adiabatic ICS for most different vibrational states, as expected. The differences between the two results are evident for low-vibrational states and gradually diminish as the vibrational quantum number increases. The difference can be ignored when ν' = 2. These observations demonstrate that nonadiabatic effects significantly influence the formation of low-vibrational products. Figure 5 shows that the curve oscillations for low-vibrational states are less pronounced in

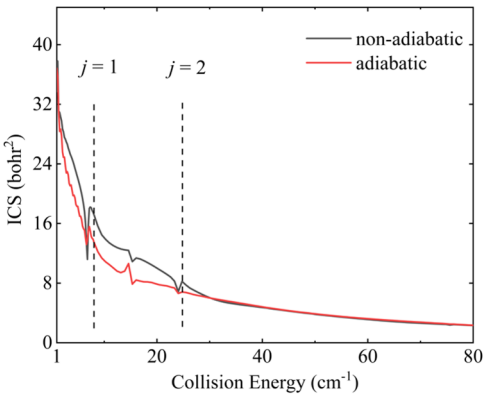

Figure 4. J = 0 cross section of the H + LiD(ν = 0, j = 0) → Li(2s) + HD reaction. Dashed lines represent the rotational-state energies of the LiD molecule.

the nonadiabatic calculations due to the shorter resonance lifetime. However, the oscillating structure is the same for different vibrational states of products in the adiabatic results, which means that these resonances occur at the entrance channel. Following our earlier study of the vibrational excitation promotion of the nonadiabatic effects at collision energies between 0.1 and 0.5 eV, we extend this investigation to lower collision energies (1−80 cm^{-1}), presenting the vibrational state distributions in Figure 6. In the adiabatic calculations, the most populated vibrational states of HD products are at ν' = 2 states, while it shifts from ν' = 2 to 3 in the nonadiabatic calculations when collision energy is higher than 50 cm^{-1}. When nonadiabatic effects are included, the production of low-vibrational states decreases significantly, resulting in a much higher abundance of highly excited vibrational products compared to low-vibrational products in nonadiabatic calculations.

In our previous work, we found that the nonadiabatic effects have no evident impact on the rotational excitation of the products in the collision energy range of 0.1−0.5 eV.[41] To study the influence of the nonadiabatic effect on the product rotational excitation in the range of 1−80 cm^{-1} collision energy, two collision energies (1 and 80 cm^{-1}) are chosen to study the rotational product distribution at different vibrational states. Figure 7 shows the product distributions at four different vibrational states when the collision energy is equal to 1 cm^{-1}. In the adiabatic calculation, products at the vibrational ground state and the first vibrational excited state are likely to stay at a low rotational state, while products are inclined to be excited to higher rotational states in the nonadiabatic calculation. For the ν' = 0 state product, the highest accessible rotational excited state is j' = 17 in the adiabatic calculation, while the highest accessible rotational excited state is j' = 19 in the nonadiabatic calculation. This change is different from the influence of the nonadiabatic effects on dynamics at 0.1−0.5 eV collision energy range. For higher vibrational states (ν' = 2 and 3), rovibrational product distributions are similar in both two calculations. These results indicate that the nonadiabatic effects have a non-negligible influence on the rotational excitation of low-vibrational products. Accessible rotational excited states gradually decrease as the vibrational quantum number increases because the internal energy shifts from rotational energy to vibrational energy. Figure 8 illustrates the rovibrational product distributions at an 80 cm^{-1} collision energy. The differences in rovibrational state distribution

https://doi.org/10.1021/acsomega.4c09864
ACS Omega 2025, 10, 5934−5942

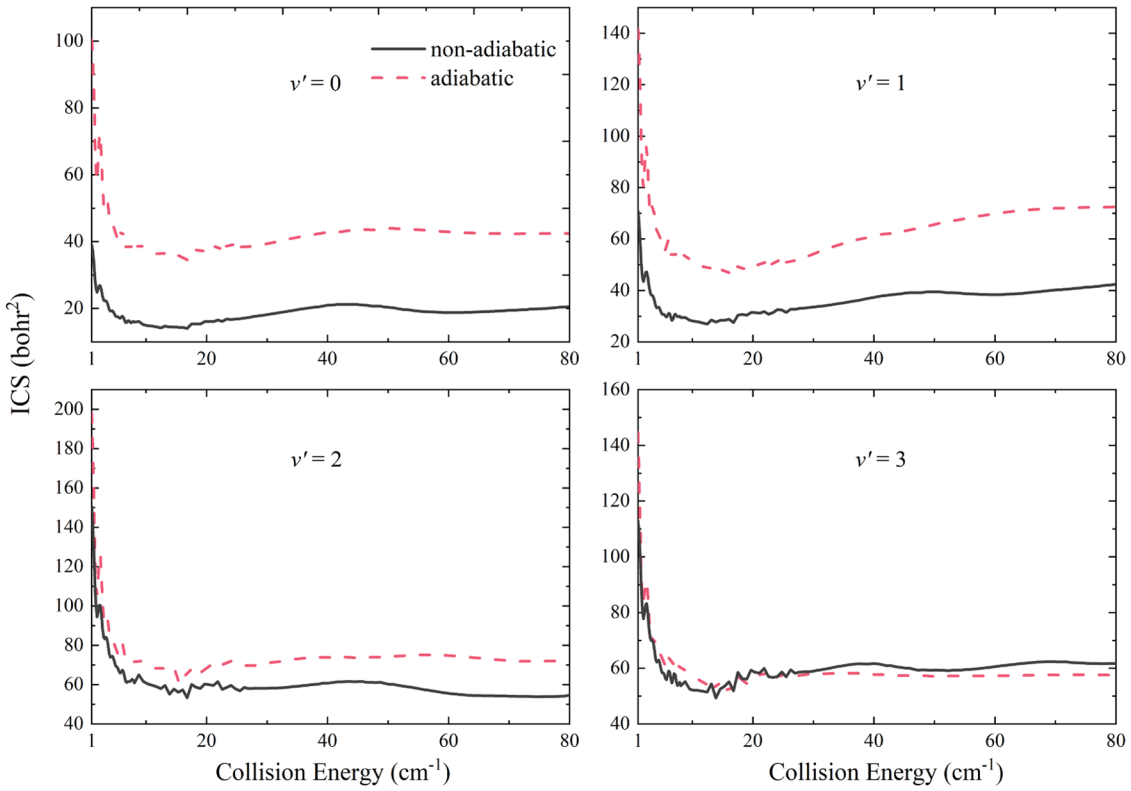

Figure 5. Vibrationally resolved ICSs of the H + LiD(v = 0, j = 0) → Li(2s) + HD reaction.

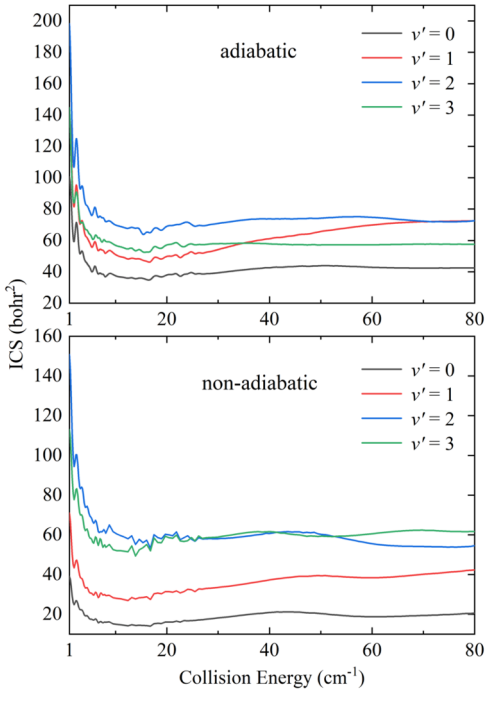

Figure 6. Adiabatic and nonadiabatic product vibrational state distribution of the H + LiD(ν = 0, j = 0) → Li(2s) + HD reactions in the range of 1−80 cm^{-1} collision energy.

between nonadiabatic and adiabatic results are also obvious when the vibrational quantum number is small. This further verifies the conclusion that the nonadiabatic effects have a great influence on the low-vibrational products. For low-vibrational states, the maximum attainable rotational excited state of the product becomes larger at 80 cm^{-1} collision energy considering the nonadiabatic effects. For some vibrational states (ν' = 0, 1, and 2) in the nonadiabatic results, the products exhibit a significant reduction in the population of intermediate rotational quantum states, while the population of highly excited rotational quantum states increases. All these analyses show that the nonadiabatic effects have a significant effect on the rotational excitation of the products in the collision energy range of 1−80 cm^{-1}.

In Figure 9, dashed and solid lines represent the adiabatic and nonadiabatic energy distribution of the product for the H + LiD → Li(2s) + HD reaction, respectively. V, T, and R represent the vibrational, translational, and rotational energy separately. Both vibrational and rotational energy increase after considering the nonadiabatic effects. Thus, the products can be excited to higher vibrational and rotational states than the results without including the nonadiabatic effects. Only the translational energy decreases when nonadiabatic effects are considered, which may influence the dynamics of the H + LiD reaction.

3.2. DCSs. DCS is a physical quantity used to describe the product's angular distribution. Its features can also reveal the reaction mechanisms in the studied reaction. The total DCS from both adiabatic and nonadiabatic calculations as a function of collision energy and scattering angle is plotted in Figure 10. Backward scattering primarily occurs at collision energies below 4 cm^{-1} for both adiabatic and nonadiabatic results, attributed to the presence of resonances. When a complex is formed in the reaction, the product angular distribution is characterized by both forward and backward scattering. The resonance contributed by J = 5 partial wave is more pronounced than other resonances; thus, the resonance lifetime is longer than other resonances. This explains why

https://doi.org/10.1021/acsomega.4c09864
ACS Omega 2025, 10, 5934−5942

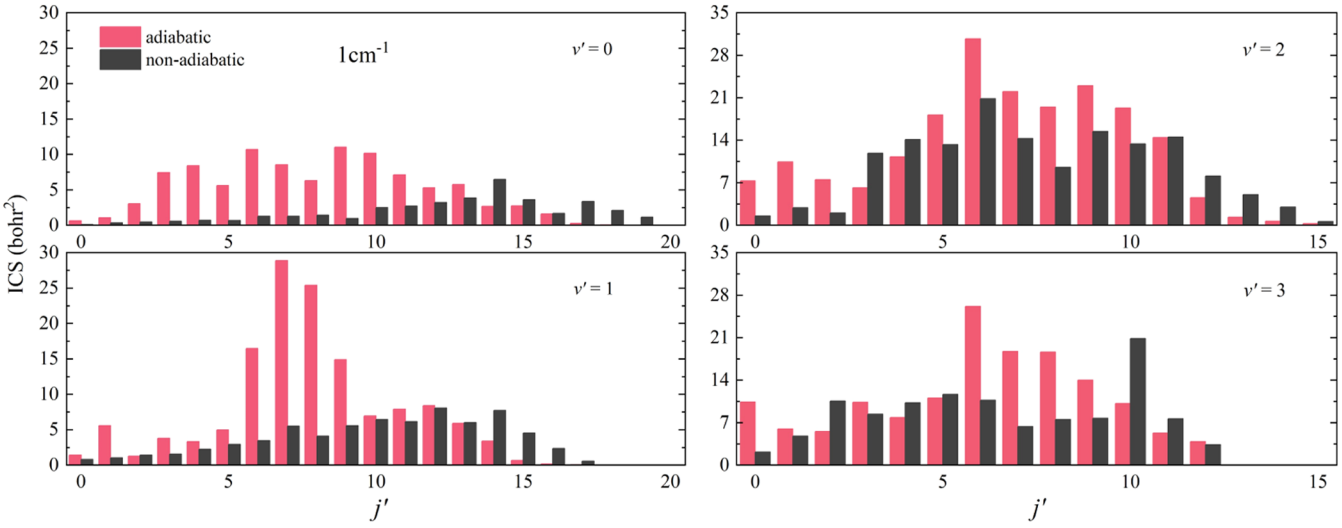

Figure 7. Product rovibrational state distribution of the H + LiD($v = 0, j = 0$) → Li(2s) + HD (v', j') reactions at 1 cm^{-1} collision energy in both representations.

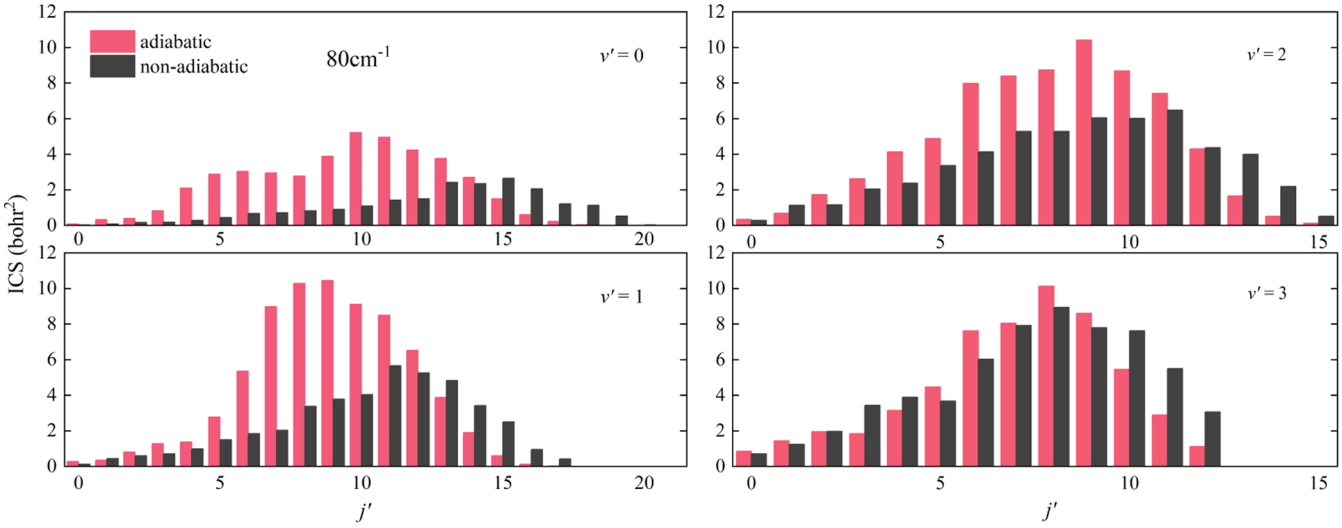

Figure 8. Product rovibrational state distribution of the H + LiD($v = 0, j = 0$) → Li(2s) + HD (v', j') reactions when collision energy is equal to 80 cm^{-1}.

the product angular distribution exhibits characteristics of both forward and backward scattering in the 1 to 4 cm^{-1} collision energy range. Both adiabatic and nonadiabatic DCS results exhibit pronounced forward scattering when the collision energy is greater than 40 cm^{-1}, which is consistent with the stripping reaction mechanism.[36] This reaction mechanism is also dominant for this reaction in the collision energy range of 0.1−0.5 eV. The characteristics of the product's angular distribution are different in the collision energy range from 4 to 40 cm^{-1} when the nonadiabatic effects are considered. Figure 10 shows that the product distribution tends to be forward scattered in the adiabatic calculations, while there is no significant population inclination in the nonadiabatic calculations.

Figures 11 and 12 show the DCSs as a function of product translational energy and scattering angle at collision energies of 1 and 80 cm^{-1}, respectively. The product translational energy increases with the radial coordinate. The vibrational states are selected from 0 to 5, and the rotational states are selected from 0 to 15. The DCS of each rovibrational state is shown as a concentric circle in Figures 11 and 12.

In Figure 11, products have no clear scattering preference in both the adiabatic and the nonadiabatic calculation. In the adiabatic results, the product angular distribution of the reaction is most prominent among the three states. The products at ($v' = 3, j' = 8$) and ($v' = 3, j' = 9$) show obvious forward scattering, while backward scattering at the ($v' = 4, j' = 4$) state is dominant. Product distributions are primarily at the ($v' = 3, j' = 10$) and ($v' = 5, j' = 0$) states in nonadiabatic results. The former exhibits backward scattering, while the latter demonstrates significant forward−backward symmetric scattering. The product distribution at 1 cm^{-1} collision energy is greatly influenced by the nonadiabatic effect. In Figure 12, the products exhibit forward scattering at a collision energy of 80 cm^{-1}, particularly in the nonadiabatic calculations, which is consistent with the stripping mechanism. In the adiabatic results, product angular distributions are prominent at the ($v' = 3, j' = 8$) state, while this state is not prominent in the nonadiabatic results. The different rovibrational product

https://doi.org/10.1021/acsomega.4c09864
ACS Omega 2025, 10, 5934−5942

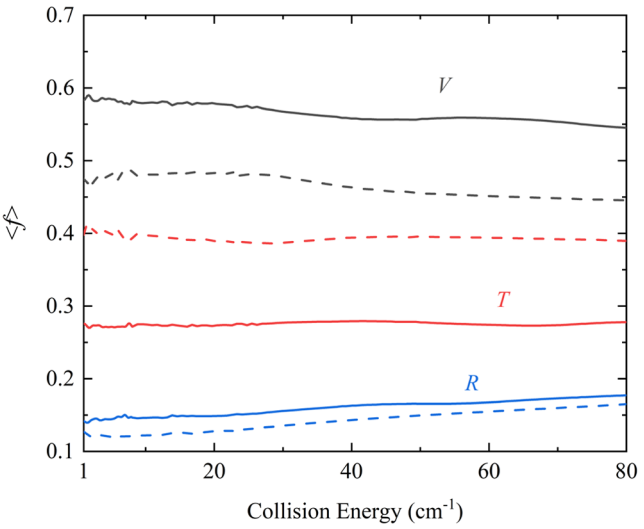

Figure 9. Dashed and solid lines represent the energy distribution of the product for H + LiD(v = 0, j = 0) → Li(2s) + HD reaction in adiabatic and nonadiabatic calculations, respectively.

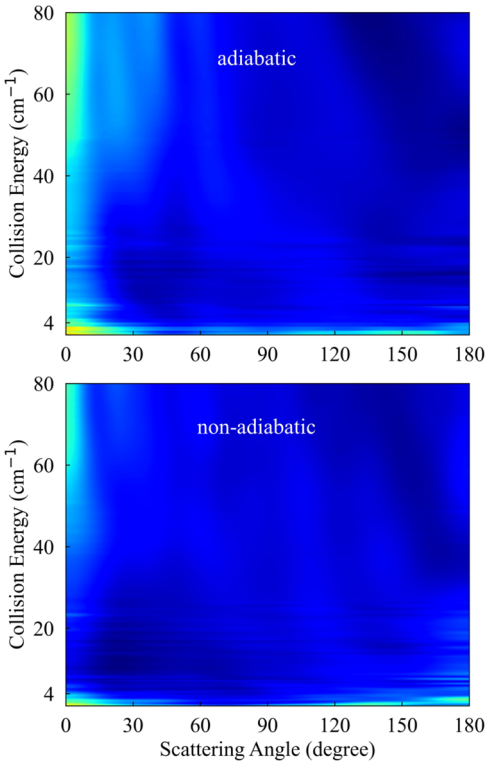

Figure 10. Total DCSs of the H + LiD(v = 0, j = 0) → Li(2s) + HD reaction in the adiabatic (top) and nonadiabatic (bottom) representations.

angular distributions indicate that the nonadiabatic effects need to be considered, especially when studying state-to-state reaction dynamics.

4. CONCLUSIONS

The TDWP method and accurate PESs are used to study the nonadiabatic effects in the H + LiD reaction over a collision energy range of 1−80 cm^{-1}. The adiabatic ICS values are found to be larger than the nonadiabatic ICS values, particularly for low-vibrational products, indicating the

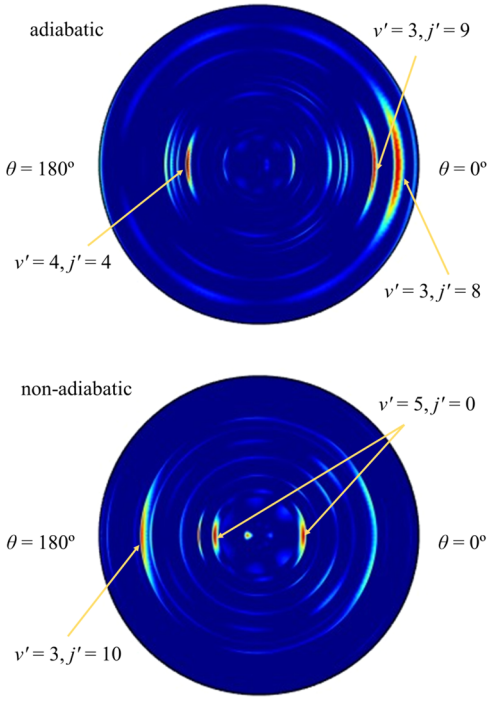

Figure 11. DCSs of the H + LiD(v = 0, j = 0) → Li(2s) + HD (v', j') reaction as a function of the product scattering angle and translational energy in polar coordinates at collision energies of 1 cm^{-1} in both representations.

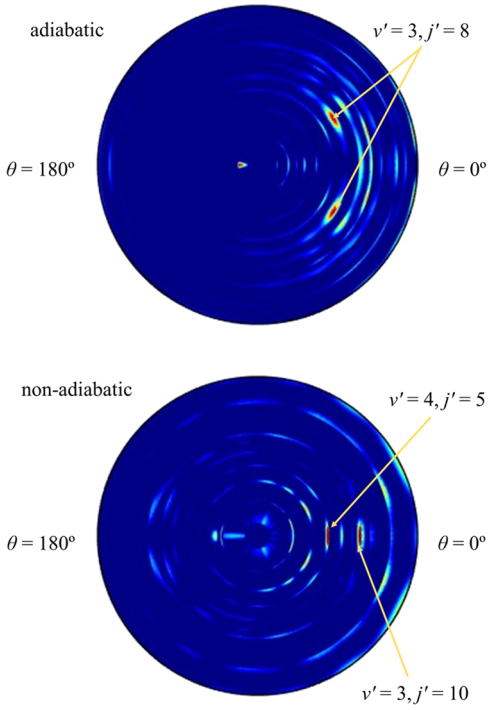

Figure 12. DCSs of the H + LiD(v = 0, j = 0) → Li(2s) + HD (v', j') reaction as a function of the product scattering angle and translational energy in polar coordinates at collision energies of 80 cm^{-1} in both representations.

significance of the nonadiabatic effects in this reaction. The resonance near the 2 cm^{-1} collision energy is contributed by the partial waves of J = 5. Rotational excitation of product is influenced by the nonadiabatic effects in the collision energy

https://doi.org/10.1021/acsomega.4c09864
ACS Omega 2025, 10, 5934−5942

range of 1−80 cm^{-1}. The DCSs suggest that the reaction mechanism is notably affected by nonadiabatic effects. Our analysis reveals the presence of multiple reaction mechanisms in this reaction, including stripping and resonance-mediated reaction mechanisms, with the stripping mechanism gradually dominating as collision energy increases. Analysis of the rovibrational state-resolved product angular distribution indicates that nonadiabatic effects play a crucial role in the title reaction. Neglecting the nonadiabatic effects, particularly when studying state-to-state reaction dynamics, may lead to erroneous conclusions. We hope that these data can provide a reference for future experiments.

AUTHOR INFORMATION

Corresponding Authors

Yuwen Bai − *School of Strengthening Basic Disciplines, Shanxi Institute of Energy, Jinzhong 030600, China;* orcid.org/0009-0004-3650-4080; Email: baiyw@sxie.edu.cn

Zijiang Yang − *School of Physics and Electronic Technology, Liaoning Normal University, Dalian 116029, China;* Email: yangzijiang@lnnu.edu.cn

Author

Bayaer Buren − *School of Science, Shenyang University of Technology, Shenyang 110870, China;* orcid.org/0000-0002-7157-5616

Complete contact information is available at: https://pubs.acs.org/10.1021/acsomega.4c09864

Notes

The authors declare no competing financial interest.

ACKNOWLEDGMENTS

This work was supported by the National Natural Science Foundation of China (No.12404301)

REFERENCES

(1) Kendrick, B. K. Quantum reactive scattering calculations for the cold and ultracold Li + LiNa → Li_2 + Na reaction. *J. Chem. Phys.* **2021**, *154* (12), No. 124303.

(2) An, F.; Chen, J. J.; Hu, X. X.; Guo, H.; Xie, D. Q. Nonadiabatic electronic energy transfer in the chemical oxygen-iodine laser: Powered by derivative coupling or spin-orbit coupling? *J. Phys. Chem. Lett.* **2020**, *11* (12), 4768−4773.

(3) Zhao, B.; Han, S. Y.; Malbon, C. L.; Manthe, U.; Yarkony, D. R.; Guo, H. Full-dimensional quantum stereodynamics of the non-adiabatic quenching of OH($A^2\sum^+$) by H_2. *Nat. Chem.* **2021**, *13* (9), 909−915.

(4) Xie, C. J.; Guo, H. Photodissociation of phenol via nonadiabatic tunneling: Comparison of two ab initio based potential energy surfaces. *Chem. Phys. Lett.* **2017**, *683*, 222−227.

(5) Xie, C. J.; Kendrick, B. K.; Yarkony, D. R.; Guo, H. Constructive and destructive interference in nonadiabatic tunneling via conical intersections. *J. Chem. Theory Comput.* **2017**, *13* (5), 1902−1910.

(6) Xie, C. J.; Zhao, B.; Malbon, C. L.; Yarkony, D. R.; Xie, D. Q.; Guo, H. Insights into the mechanism of nonadiabatic photodissociation from product vibrational distributions. The remarkable case of phenol. *J. Phys. Chem. Lett.* **2020**, *11* (1), 191−198.

(7) An, H.; Baeck, K. K. Practical and reliable approximation of nonadiabatic coupling terms between triplet electronic states using only adiabatic potential energies. *Chem. Phys. Lett.* **2018**, *696*, 100−105.

(8) Zhang, P. Y.; Han, K. L. Adiabatic/nonadiabatic state-to-state reactive scattering dynamics implemented on graphics processing units. *J. Phys. Chem. A* **2013**, *117* (36), 8512−8518.

(9) Kendrick, B. K.; Balakrishnan, N. Geometric phase effects in ultracold chemical reactions. *Atoms* **2019**, *7* (3), No. 65.

(10) Yuan, D. F.; Guan, Y. F.; Chen, W. T.; Zhao, H. L.; Yu, S. R.; Luo, C.; Tan, Y. X.; Xie, T.; Wang, X. G.; Sun, Z. G.; Zhang, D. H.; Yang, X. M. Observation of the geometric phase effect in the H + HD → H_2 + D reaction. *Science* **2018**, *362* (6420), 1289−1293.

(11) Bouakline, F.; Althorpe, S. C.; Ruiz, D. P. Strong geometric-phase effects in the hydrogen-exchange reaction at high collision energies. *J. Chem. Phys.* **2008**, *128* (12), No. 124322.

(12) Xie, Y. R.; Zhao, H. L.; Wang, Y. F.; Huang, Y.; Wang, T.; Xu, X.; Xiao, C. L.; Sun, Z. G.; Zhang, D. H.; Yang, X. M. Quantum interference in H + HD → H_2 + D between direct abstraction and roaming insertion pathways. *Science* **2020**, *368* (6492), 767−771.

(13) Juanes-Marcos, J. C.; Althorpe, S. C. Geometric phase effects in the H+H reaction: Quantum wave-packet calculations of integral and differential cross sections. *J. Chem. Phys.* **2005**, *122* (20), No. 204324.

(14) Yuan, D. F.; Chen, W. T.; Luo, C.; Tan, Y. X.; Li, S. H.; Huang, Y.; Sun, Z. G.; Yang, X. M.; Wang, X. A. Imaging the state-to-state dynamics of the H + D_2 → HD + D reaction at 1.42 eV. *J. Phys. Chem. Lett.* **2020**, *11* (4), 1222−1227.

(15) Yuan, D. F.; Yu, S. R.; Chen, W. T.; Sang, J. W.; Luo, C.; Wang, T.; Xu, X.; Casavecchia, P.; Wang, X. A.; Sun, Z. G.; Zhang, D. H.; Yang, X. M. Direct observation of forward-scattering oscillations in the H + HD → H_2 + D reaction. *Nat. Chem.* **2018**, *10* (6), 653−658.

(16) Kendrick, B. K.; Hazra, J.; Balakrishnan, N. Geometric phase effects in the ultracold H + H_2 reaction. *J. Chem. Phys.* **2016**, *145* (16), No. 164303.

(17) Kendrick, B. K.; Hazra, J.; Balakrishnan, N. Geometric phase effects in the ultracold D + HD → D + HD and D + HD ↔ H + D_2 reactions. *New J. Phys.* **2016**, *18* (12), No. 123020.

(18) Kendrick, B. K.; Hazra, J.; Balakrishnan, N. The geometric phase controls ultracold chemistry. *Nat. Commu.* **2015**, *6*, No. 7918.

(19) Kendrick, B. K.; Hazra, J.; Balakrishnan, N. Geometric phase appears in the ultracold hydrogen exchange reaction. *Phys. Rev. Lett.* **2015**, *115* (15), No. 153201.

(20) Son, H.; Park, J. J.; Lu, Y. K.; Jamison, A. O.; Karman, T.; Ketterle, W. Control of reactive collisions by quantum interference. *Science* **2022**, *375* (6584), 1006−1010.

(21) Nichols, M. A.; Liu, Y. X.; Zhu, L. B.; Hu, M. G.; Liu, Y.; Ni, K. K. Detection of long-lived complexes in ultracold atom-molecule collisions. *Phys. Rev. X* **2022**, *12* (1), No. 011049.

(22) Li, W. T.; Wang, X. M.; Zhao, H. L.; He, D. Non-adiabatic dynamics studies of the K($4p^2P$) + H_2($X^1\sum_g^+$) reaction based on new diabatic potential energy surfaces. *Phys. Chem. Chem. Phys.* **2020**, *22* (28), 16203−16214.

(23) Hsiao, Y. C.; Liu, D. K.; Fung, H. S.; Lin, K. C. Temperature effect on the deactivation of electronically excited potassium by hydrogen molecule. *J. Chem. Phys.* **2000**, *113* (11), 4613−4619.

(24) Yuan, J. C.; Duan, Z. X.; Wang, S. F.; Liu, J. Y.; Han, K. L. Significant effects of vibrational excitation of reactant in K + H_2 → H + KH reaction based on a new neural network potential energy surface. *Phys. Chem. Chem. Phys.* **2018**, *20* (31), 20641−20649.

(25) Buren, B.; Yang, Z. J.; Chen, M. D. Dynamics study on the non-adiabatic Na(3p) + HD → NaH/NaD + D/H reaction: insertion−abstraction mechanism. *Phys. Chem. Chem. Phys.* **2020**, *22* (6), 3633−3642.

(26) Buren, B.; Yang, Z. J.; Chen, M. D. Non-adiabatic state-to-state dynamic studies of Na(3p) + H_2(v = 1, 2, 3; j = 0) → NaH + H reactions. *Chem. Phys. Lett.* **2019**, *723*, 128−132.

(27) Wang, S. F.; Yang, Z. J.; Yuan, J. C.; Chen, M. D. New diabatic potential energy surfaces of the NaH_2 system and dynamics studies for the Na(3p) + H_2 → NaH + H reaction. *Sci. Rep.* **2018**, *8*, No. 17960.

(28) Chang, Y. P.; Hsiao, M. K.; Liu, D. K.; Lin, K. C. Rotational and vibrational state distributions of NaH in the reactions of Na($4\,^2S$, $3\,^2D$, and $6\,^2S$) with H_2: Insertion versus harpoon-type mechanisms. *J. Chem. Phys.* **2008**, *128* (23), No. 234309.

(29) Yin, R. L.; Gao, N.; Cao, J.; Li, Y. C.; Wang, D. Q.; Huang, X. R. Global accurate diabatic potential surfaces for the reaction H + Li_2. *RSC Adv.* **2020**, *10* (64), 39226−39240.

(30) Song, J. M.; Zhu, Z. L. Dynamics studies of the Li(^{2}S) + H_2($X^1\sum_g^+$) → LiH ($X^1\sum^+$) + H(^{2}S) reaction by time-dependent wave packet and quasi-classical trajectory methods. *Comput. Theor. Chem.* **2020**, *1173*, No. 112703.
(31) Bai, Y. W.; Buren, B.; Yang, Z. J.; Chen, M. D. Time-dependent wave packet dynamics study of non-adiabatic Li(2p) + HD → LiH/LiD + D/H reaction in a diabatic representation. *Chem. Phys. Lett.* **2021**, *764*, No. 138279.
(32) He, D.; Yuan, J. C.; Chen, M. D. Influence of rovibrational excitation on the non-diabatic state-to-state dynamics for the Li(2p) + H_2 → LiH + H reaction. *Sci. Rep.* **2017**, *7*, No. 3084.
(33) Fu, L. W.; Wang, D. Q.; Huang, X. R. Accurate potential energy surfaces for the first two lowest electronic states of the Li(2p) + H_2 reaction. *RSC Adv.* **2018**, *8* (28), 15595−15602.
(34) He, D.; Li, W. T.; Wang, M. S. A study on the non-adiabatic dynamics of the Li(2p) + H_2 → Li(2s) + H_2 quenching reaction calculated by time-dependent wavepacket method. *Chem. Phys. Lett.* **2021**, *780*, No. 138910.
(35) Martínez, T. J. Ab initio molecular dynamics around a conical intersection: Li(2p) + H_2. *Chem. Phys. Lett.* **1997**, *272* (3−4), 139−147.
(36) He, X.; Wu, H.; Zhang, P.; Zhang, Y. Quantum state-to-state dynamics of the H + LiH → H_2 + Li reaction. *J. Phys. Chem. A* **2015**, *119* (33), 8912−8921.
(37) Wang, X. L.; Zheng, Y. J.; Yang, H. Effects of rovibrational excitation of LiH on the LiH depletion and H exchange channels for the reaction H(^{2}S) + LiH($X^1\sum^+$) on a new potential energy surface. *Chem. Phys. Lett.* **2020**, *740*, No. 137043.
(38) Padmanaban, R.; Mahapatra, S. Time-dependent wave packet dynamics of the H+HLi reactive scattering. *J. Chem. Phys.* **2002**, *117* (14), 6469−6477.
(39) Li, W. T.; Sun, J. X.; He, D. Non-adiabatic dynamics studies of the H(^{2}S) + LiH($X^1\sum^+$) reaction by time-dependent wave packet method. *Phys. Chem. Chem. Phys.* **2020**, *22* (31), 17587−17596.
(40) Li, W. T.; Cui, L. L.; Xing, W.; Wang, J. M. State-to-state rate constants for the H + LiH(v_0 = 0, j_0 = 0) reaction: An accurate nonadiabatic dynamical study. *Astrophys. J.* **2021**, *915* (2), No. 104.
(41) Bai, Y. W.; Yang, Z. J.; Buren, B.; Mao, Y.; Chen, M. D. Quantum dynamics studies on the non-adiabatic effects of H plus LiD reaction. *Front. Phys.* **2023**, *18* (3), No. 31303.
(42) He, D.; Yuan, J. C.; Li, H. X.; Chen, M. D. Global diabatic potential energy surfaces and quantum dynamical studies for the Li(2p) + H_2($X^1\sum_g^+$) → LiH($X^1\sum^+$) + H reaction. *Sci. Rep.* **2016**, *6*, No. 25083.
(43) Bircher, M. P.; Liberatore, E.; Browning, N. J.; Brickel, S.; Hofmann, C.; Patoz, A.; Unke, O. T.; Zimmermann, T.; Chergui, M.; Hamm, P.; Keller, U.; Meuwly, M.; Woerner, H. J.; Vanicek, J.; Rothlisberger, U. Nonadiabatic effects in electronic and nuclear dynamics. *Struct. Dyn.* **2017**, *4* (6), No. 061510.
(44) Buren, B.; Chen, M. D. Stereodynamics-controlled product branching in the nonadiabatic H + NaD → Na(3s, 3p) + HD reaction at low temperatures. *J. Phys. Chem. A* **2022**, *126* (16), 2453−2462.
(45) Boggio-Pasqua, M.; Voronin, A. I.; Halvick, P.; Rayez, J. C.; Varandas, A. J. C. Coupled potential energy surfaces for the two lowest ^{2}A′ electronic states of the C_2H molecule. *Mol. Phys.* **2000**, *98* (23), 1925−1938.
(46) Yarkony, D. R. On the construction of diabatic bases using molecular properties. Rigorous results in the vicinity of a conical intersection. *J. Phys. Chem. A* **1998**, *102* (42), 8073−8077.
(47) Sun, Z. G.; Lee, S. Y.; Guo, H.; Zhang, D. H. Comparison of second-order split operator and Chebyshev propagator in wave packet based state-to-state reactive scattering calculations. *J. Chem. Phys.* **2009**, *130* (17), No. 174102.
(48) Berteloite, C.; Lara, M.; Bergeat, A.; Le Picard, S. D.; Dayou, F.; Hickson, K. M.; Canosa, A.; Naulin, C.; Launay, J. M.; Sims, I. R.; Costes, M. Kinetics and dynamics of the S(^{1}D$_2$) + H_2 → SH + H reaction at very low temperatures and collision energies. *Phys. Rev. Lett.* **2010**, *105* (20), No. 203201.
(49) Mao, Y.; Buren, B.; Yang, Z. J.; Chen, M. D. Time-dependent wave packet dynamics study of the resonances in the H + LiH^+(v = 0, j = 0) → Li^+ + H_2 reaction at low collision energies. *Phys. Chem. Chem. Phys.* **2022**, *24* (25), 15532−15539.

https://doi.org/10.1021/acsomega.4c09864
ACS Omega 2025, 10, 5934−5942